Hydrol. Earth Syst. Sci. Discuss., 10, 4463–4487, 2013
www.hydrol-earth-syst-sci-discuss.net/10/4463/2013/
doi:10.5194/hessd-10-4463-2013

Hydrology and Earth System Sciences
Open Access
Discussions

Representation of water abstraction from a karst conduit with numerical discrete-continuum models

T. Reimann[1], M. Giese[2], T. Geyer[2], R. Liedl[1], J. C. Maréchal[3], and W. B. Shoemaker[4]

[1]Institute for Groundwater Management, TU Dresden, Dresden, Germany
[2]Geoscientific Centre, University of Göttingen, Göttingen, Germany
[3]Bureau de Recherche Géologique Minière (B.R.G.M.), Montpellier, France
[4]8307 Balgowan Road, Miami Lakes, FL 33016, USA

Received: 20 February 2013 – Accepted: 13 March 2013 – Published: 8 April 2013

Correspondence to: T. Reimann (thomas.reimann@tu-dresden.de)

Published by Copernicus Publications on behalf of the European Geosciences Union.

Abstract

Karst aquifers are characterized by highly conductive conduit flow paths embedded in a less conductive fissured and fractured matrix resulting in strong permeability contrasts with structured heterogeneity and anisotropy. Groundwater storage occurs predominantly in the fissured matrix. Hence, most karst models assume quasi steady-state flow in conduits neglecting conduit associated drainable storage (CADS). The concept of CADS considers storage volumes, where karst water is not part of the active flow system but rather hydraulically connected to conduits (for example karstic voids and large fractures). The disregard of conduit storage can be inappropriate when direct water abstraction from karst conduits occurs, e.g. large scale pumping. In such cases, CADS may be relevant. Furthermore, the typical fixed head boundary condition at the karst outlet can be inadequate for water abstraction scenarios because unhampered water inflow is possible. The objective of this paper is to analyze the significance of CADS and flow-limited boundary conditions on the hydraulic behavior of karst aquifers in water abstraction scenarios. To this end, the numerical hybrid model MODFLOW-2005 Conduit Flow Process Mode 1 (CFPM1) is enhanced to account for CADS. Additionally, a fixed-head limited-flow (FHLQ) boundary condition is added that limits inflow from constant head boundaries to a user-defined threshold. The affect and proper functioning of these modifications is demonstrated by simplified model studies. Both enhancements, CAD storage and the FHLQ boundary, are shown to be useful for water abstraction scenarios within karst aquifers. An idealized representation of a large-scale pumping test in a karst conduit is used to demonstrate that the enhanced CFPM1 is potentially able to adequately represent water abstraction processes in both the conduits and the matrix of real karst systems.

1 Introduction

Karst aquifers can be described as triple porosity systems with continuous primary porosity in the matrix, secondary porosity within fissures and fractures, and tertiary porosity represented by solution enlarged features, i.e. highly permeable conduits (e.g. Worthington et al., 2000). Strong permeability contrasts within triple porosity systems lead to uncertainties during characterization of these systems with conventional empirical, analytical, and numerical methods. For example, artificial tracer tests are suitable methods for characterization of large karst conduit systems, e.g. Atkinson et al. (1973). However, tracer methods fail to characterize matrix properties on a catchment scale. In contrast, conventional hydraulic borehole tests provide useful information about local aquifer properties but also are unable to determine hydraulic information on catchment scale because of, for example, limited pumping rates. Only a few experiments are documented that address large scale characterization of karst aquifers. In particular, Maréchal et al. (2008) performed a pumping test with abstraction rates up to several hundred liters per second for about one month. These high abstraction rates were possible because the pumping well was directly connected to the conduit system. Consequently, this pumping test produced drawdowns in both the conduit system and the matrix and, therefore, provided evidence to infer the existence of large water storages within the matrix and the conduits (Maréchal et al., 2008), see Fig. 1.

Different matrix and conduit storage concepts in karst aquifers are presented in literature (Bakalowicz, 2005). Depending on the particular karst system, several double porosity concepts are commonly applied. Mangin (1975, 1994) associated large water storage to poorly interconnected large voids in the adjacent rock of conduit systems, which transmit water from the groundwater table towards a spring (annex systems to drainage). Mangin (1975, 1994) further assumes that matrix storage is negligible. In contrast, Drogue (1974, 1992) proposed areal water storage in the hydraulically continuous matrix drained by the highly permeable karst conduit system. Storage directly associated with discrete conduits was not considered. However, the existence of water

storage within highly permeable karst structures is known from speleological investigations (Ford and Williams, 2007; Mangin, 1975) and karst hydraulics (Geyer et al., 2008; Maréchal et al., 2008). Worthington et al. (2000) and Worthington (2007) presented field studies that clearly emphasize the necessity to describe karst aquifers as triple porosity systems.

Hybrid models, which couple a discrete pipe flow model to a continuum model, represent a suitable approach to simulate karst aquifers (Sauter et al., 2006). Liedl et al. (2003) developed a hybrid modeling approach for the simulation of laminar and turbulent pipe flow coupled to a matrix continuum. Shoemaker et al. (2008) incorporated this hybrid model approach within MODFLOW-2005 as the Conduit Flow Process Mode 1 (CFPM1). Laminar groundwater flow in the continuum model is represented by the Darcy equation

$$\frac{\delta}{\delta x}(K_{xx}\frac{\delta h}{\delta x}) + \frac{\delta}{\delta y}(K_{yy}\frac{\delta h}{\delta y}) + \frac{\delta}{\delta z}(K_{zz}\frac{\delta h}{\delta z}) \pm W = S_s(\frac{\delta h}{\delta t}) \quad (1)$$

with K hydraulic conductivity along the x, y, and z-axes [$L\,T^{-1}$], h head [L], W volumetric flux per unit volume [T^{-1}], S_s specific storage [L^{-1}] and t time [T] (McDonald and Harbaugh, 1988). Laminar pipe flow is represented by the Hagen-Poiseuille equation

$$Q = -\frac{\pi d^4 g \Delta h}{128 \upsilon \Delta l} \quad (2)$$

with d pipe diameter [L], g gravitational acceleration [$L\,T^{-2}$], υ kinematic viscosity of water [$L^2\,T^{-1}$] , and l length of pipe [L] (Shoemaker et al., 2008). Turbulent pipe flow is considered by the Colebrook-White equation

$$Q = -\sqrt{\frac{|\Delta h| g d^5 \pi^2}{2\Delta l}} \log\left(\frac{2.51\upsilon}{\sqrt{\frac{2|\Delta h| g d^3}{\Delta l}}} + \frac{k_c}{3.71 d}\right)\frac{\Delta h}{|\Delta h|} \quad (3)$$

with k_c mean roughness height [L] (Shoemaker et al., 2008). The coupling between pipe network and continuum model is realized through a head dependent exchange flow rate Q_{ex}

$$Q_{ex} = \alpha_{ex}(h_{conduit} - h_{matrix}) \quad (4)$$

where $h_{conduit}$ [L] is the conduit head, h_{matrix} [L] is the matrix head, and α_{ex} [$L^2\,T^{-1}$] is the pipe conductance (Barenblatt et al., 1960; Shoemaker et al., 2008). However, these hybrid models fail to simulate transient water storage within the conduit system because steady state pipe flow equations are applied, i.e. drainable conduit storage is not considered. For this reason, transient water storage can be considered by the continuum model only. Following this, Reimann et al. (2011) presented a modeling approach to simulate unsteady discrete flow in a variably filled pipe network coupled to a matrix continuum. The approach is suitable for fundamental studies but potential drawbacks are the high parameter demand and the high computational effort.

The objective of this article is to provide a distributive process-based modeling approach that allows the simulation of hydraulic impacts (discharge events, large scale hydraulic tests) on karst systems with manageable data demand under consideration of important storage processes. For that reason, the hybrid modeling approach of CFPM1 was further enhanced by Conduit-Associated Drainable Storage (CADS). Scenarios with water abstraction from the conduits can result in a reversion of the flow direction, i.e. inflow at the karst spring (e.g. Maréchal et al., 2008). Hence, the numerical model needs to be complemented by constrained boundary conditions to avoid unhampered water inflow through the spring. The performance of the numerical model is evaluated by synthetic scenarios. Subsequently, an idealized model represents the large scale pumping test (Maréchal et al., 2008), whereas model results are qualitatively compared with the field measurements.

2 Enhanced concept and technical implementation into modflow-2005 conduit flow process

2.1 Conduit-Associated Drainable Storage (CADS)

To consider drainable conduit storage within CFP Mode 1, the conduit associated drainable storage package (CADS) was developed. Conceptually, CAD storage is assumed

to be in direct hydraulic contact with draining conduits, see Fig. 2, so that

$$h_{conduit} = h_{CADS} \tag{5}$$

where h_{CADS} is the head [L] in the CAD storage. The CAD storage is conceptualized as a rectangular block directly associated with the conduit, i.e. the CADS base area is the conduit length times the width of the CAD storage (Fig. 2). Finally, the volume of the CADS is computed as

$$V_{CADS} = L_{CADS} W_{CADS} (h_{CADS} - z_{bottom}); \tag{6}$$

$$h_{CADS} > z_{bottom}$$

where L_{CADS} is the length [L] (= conduit length), W_{CADS} is the width of the CAD storage [L], and z_{bottom} is the elevation of the conduit bottom [L]. The ratio V_{CADS}/h_{CADS} corresponds to the free-surface area of the dewatering conduit network defined by Maréchal et al. (2008). It is assumed that water released from the CADS due to head variations immediately enters the conduit resulting in additional discharge. The resulting discharge from CADS storage, Q_{CADS} [$L^3\,T^{-1}$], is considered as

$$Q_{CADS} = \frac{V_t - V_{(t-\Delta t)}}{\Delta t} \tag{7}$$

where V_t is the volume of the CAD storage [L^3] at the time t and Δt is the time step size [T]. Q_{CADS} is directly added to the CFPM1 system of equations and subsequently considered for the iterative solution whereas negative Q_{CADS} indicates that flow is from the CADS into the conduits.

2.2 Constrained fixed head boundary condition

A conduit with a fixed head boundary condition can strongly affect in- or outflow of the highly permeable pipe network at the outlet, i.e. a karst spring. For example, water abstraction from a distinctive and well-developed conduit network can result in unlimited

water inflow through a fixed head boundary. However, this contradicts the drawdown behavior in field situations, e.g. Maréchal et al. (2008) (Fig. 1). The fixed head limited flow (FHLQ) boundary condition is intended to limit inflow for constant head boundaries. If a user defined discharge threshold is exceeded, the fixed head boundary condition switches to a fixed flow boundary condition, which results in a variable head (Bauer et al., 2005):

$$\text{FHLQ} = \begin{cases} h_{\text{conduit}} = H, & Q \le Q_{\text{L}} \\ Q = Q_{\text{L}}, & \text{else} \end{cases} \quad (8)$$

with H fixed head value (FH) [L], Q discharge at the boundary (negative values denote outflow) [$L^3\,T^{-1}$], and Q_L limiting discharge (LQ) [$L^3\,T^{-1}$]. H and Q_L are to be defined by the user according to site-specific conditions.

3 Test cases

The functionality of the enhanced CFPM1 was verified with a simple test setup, which is subsequently described.

3.1 Model setup

The basic model setup consists of a continuum model with 11 columns and 11 rows whereas each cell is 100 m × 100 m (Fig. 3). Hydraulic conductivity and storage coefficient of the matrix continuum are set as $K_m = 1 \times 10^{-5}\,m\,s^{-1}$ and $S_m = 0.01$, respectively. The embedded conduit consists of 6 nodes connected by 5 conduits (each 100 m long). The conduit diameter is 0.5 m and for a modified model run is increased to 2.5 m. Conduit roughness is set to 0.01 m. Water transfer between conduits and matrix is parameterized by a fixed water transfer coefficient per unit length $\alpha_{ex}/L_{conduit} = 1 \times 10^{-5}\,m\,s^{-1}$. All lateral outer boundaries of the matrix continuum are of Neumann type (no-flow). Diffuse areal recharge is uniformly applied to the continuum and direct point recharge is applied to conduit node 1 (Fig. 3). The karst spring is

represented by a fixed head of 50 m at conduit node 6. Water abstraction is realized by negative direct recharge in node 5. The model simulates three periods, specifically: (1) pre-pumping from 0 to 86 400 s; (2) pumping from 86 400 to 172 800 s at rates of 0.5, 1.0, and 1.5 $m^3\,s^{-1}$, respectively, and (3) recovery from 172 800 to 345 600 s.

3.2 Results for the basic model (available CFPM1)

For stress period 1, spring discharge equaled 0.2 $m^3\,s^{-1}$ and consisted of diffuse areal recharge (0.1 $m^3\,s^{-1}$) plus direct point recharge to the conduit (0.1 $m^3\,s^{-1}$ at node 1, see Fig. 3). Water abstraction by pumping in period 2 results in immediate variation of spring discharge whereas a quasi-steady conduit head is reached. Subsequently, this quasi-steady conduit head is only slightly altered by the variation of matrix heads (Fig. 4). As the pumping rate exceeds diffuse and direct recharge, water inflow through the fixed head boundary at node 6 occurs (Fig. 4). Further, pumping-induced discharge in conduits results in a change of conduit heads that depends on the hydraulic capacity of the conduit, i.e. the conduit diameter and roughness. For the investigated (basic) setting the used conduit diameter of 0.5 m was found to be hydraulically limiting resulting in noticeable head loss along the conduit and, therefore, clearly marked drawdown at the pumping well (Fig. 4). In case of such a hydraulically constrained conduit, water transfer from the matrix is increased to provide water for pumping.

The basic scenario was modified by increasing the conduit diameter to 2.5 m. For this setting, the drawdown of conduit head during pumping can be neglected indicating that the conduit hydraulics are not limiting. Basically unhampered water inflow through the fixed head boundary can occur (Fig. 4). After pumping is stopped, conduit heads immediately rise up to pre-pumping values (drawdown = 0 m, see Fig. 4).

3.3 Results for CFPM1 with CADS

The basic model setup (previous section) creates immediate drawdown due to pumping because of the steady-state hydraulic approach used for the conduits, which neglects

dynamic processes like inertia and momentum forces and does not consider storage. It can be assumed that steady-state hydraulics are sufficient to represent flow processes in the conduits on a relatively long time scale, e.g. pumping for several hours, where the initial imbalance is not significant. However, when matching drawdowns for relatively short time-scale pumping tests, CAD may be necessary.

The initial model was enhanced by adding CAD storage directly linked with the conduit system. For this model run, the CADS width was set to 0.5 m resulting in roughly 5000 m^3 CADS (assuming $h_{conduit} = h_{CADS} = 50$ m with a node elevation of 30 m). Subsequently, model runs for the 0.5 m diameter conduit were repeated because this setup results in a significant drawdown (Fig. 4), which is necessary to induce CADS changes.

It is obvious that CAD storage results in a significantly delayed drawdown (Fig. 5 left) because the water level depression due to pumping stimulates water release and therewith additional discharge from CADS draining. This effect is also shown by the initial damping of spring inflow (Fig. 5 left). It can be concluded that CFPM1 with CADS is able to reproduce the characteristic damped drawdown behavior within conduits in cases of short and long-term water abstraction (compare Fig. 1).

3.4 Results for CFPM1 with FHLQ boundary condition

The basic model run demonstrated that in cases of unlimited conduit hydraulics, e.g. for sufficiently large conduits, unhampered water inflow through the fixed head boundary occurs (Fig. 4). Subsequently, the drawdown is very minor and potential CAD storage does not become significant. The fixed head limited flow (FHLQ) boundary condition can constrain inflow through the fixed head boundary resulting in limited inflow to the conduit system. To investigate this behavior, a pumping rate of 0.25 $m^3 s^{-1}$ was applied (node 5) and the fixed head boundary condition of the basic model setup was extended by a flow constraint of 0.025 $m^3 s^{-1}$ water inflow (node 6, compare Fig. 3). Consequently, the water deficit of 0.05 $m^3 s^{-1}$ (0.20 $m^3 s^{-1}$ recharge minus 0.25 $m^3 s^{-1}$ water abstraction) is balanced out by spring inflow not exceeding 0.025 $m^3 s^{-1}$ and additional water transfer from the continuum matrix of 0.025 $m^3 s^{-1}$ (50 % of the deficit

each). Results for both conduits with 0.5 m and 2.5 m diameter are presented in Fig. 5 right. Hence, it is apparent that the FHLQ boundary limits the conduit inflow, which is more or less equal for both conduits because discharge is not limited by conduit hydraulics, and therefore drawdown is less sensitive to the conduit diameter. As the spring inflow is constrained by the FHLQ boundary (see Fig. 5 right), the water deficit inside the conduit system caused by pumping is balanced out by water transfer from the matrix. Hence, conduit heads (and therefore drawdown) are more strongly related to matrix hydraulic properties (e.g. storage).

3.5 Results for CFPM1 with CADS and FHLQ boundary condition

Next, both CADS and FHLQ are tested in parallel. As in the previous section, inflow to the karst system through the spring was limited to 0.025 $m^3 s^{-1}$ by using the FHLQ boundary condition. For a first scenario, the influence of the pumping rate on conduit drawdown was investigated. The CADS width was set to 0.25 m. In a second scenario the CADS width and therewith the CADS volume were varied while the pumping rate was fixed to 0.30 $m^3 s^{-1}$. Model runs were performed with conduit diameters equal to $D = 0.5$ m and $D = 2.5$ m resulting in a very similar behavior. Hence, only findings for the $D = 0.5$ m conduit are presented in detail.

Outcomes for the first scenario with varying pumping rates are presented in Fig. 6 (left). The well drawdown is very sensitive to the pumping rate. Water release from the CAD storage results in the characteristic, damped drawdown behavior at the conduit pumping well. Because the inflow into the conduit system is hydraulically constrained, i.e. by the FHLQ boundary condition as well as by matrix exchange, the long term abstraction rate is limited by a threshold value, which, if the threshold is exceeded, creates dry conduits. For the example setting, this threshold is slightly higher than 0.30 $m^3 s^{-1}$ (Fig. 6 left; the conduit bottom is reached by a drawdown of approximately 20 m).

Findings for the scenario with variable CADS width are shown in Fig. 6 (right). An increased CADS results in less pronounced drawdown because the water demand due

to abstraction is balanced out by inflow (storage release) from the CADS. Furthermore, the increased CADS lengthens recovery times if water abstraction stops (Fig. 6 right). It follows that the CADS volume can be calibrated during transient conditions.

4 Case study

4.1 Model setup

A highly idealized representation of the field situation described by Maréchal et al. (2008) was created for further CADS and FHLQ testing. This case study tests the ability of CFPM1 to qualitatively reproduce the hydraulic behavior observed in the field. Data and parameters used for this idealized model are, in most instances, from Maréchal et al. (2008). A sketch of the study area and the model are shown in Fig. 7 (compare also Fig. 1). The matrix continuum is discretized by 85 rows and 35 columns with cell lengths and widths equal to 100 m × 100 m. Vertically, the model is represented by one unconfined layer with top = 250 m a.s.l. and bottom = −150 m a.s.l. Cauchy boundaries are applied at the north and south borders of the model grid to represent streams in the catchment area. The head dependent water transfer between matrix and rivers is approximated with the River Package whereas the riverbed conductance was set to $100\,m^2\,s^{-1}$ (Fig. 7). All other lateral outer boundaries are of Neumann type (no flow). A uniform diffuse areal recharge of $6.34 \times 10^{-9}\,m^3\,m^{-2}\,s^{-1}$ ($200\,mm\,a^{-1}$) is applied. The matrix hydraulic conductivity K_m is set to $9 \times 10^{-6}\,m\,s^{-1}$ (calibrated to matrix hydraulic heads) and matrix storage is $S_m = 0.007$ (compare with Maréchal et al., 2008).

Highly conductive karst features are represented by one central conduit from north to south, which is subdivided into 90 tubes (each approximately 100 m long) and 91 nodes. CADS is implemented with a storage width of $W_{CADS} = 0.21$ m resulting in a storage area $W_{CADS} \times L_{CADS}$ of $\sim 1900\,m^2$ (Maréchal et al., 2008). Conduit node elevation is at 0 m a.s.l. The conduit diameter is estimated from spring response analysis to be 3.5 m (Birk and Geyer, 2006) according to the concept of Ashton (1966). Pipe

roughness is set to 0.01 m. Water transfer between matrix and conduit is realized by setting $\alpha_{ex}/L_{conduit}$ to $4.5 \times 10^{-7}\,m\,s^{-1}$. The water transfer coefficient α_{ex} is doubled in node 1 and node 91 to represent the coupling between river and conduit. The karst spring in the south (node 91) is implemented by an FHLQ boundary condition with fixed head at 76.9 m a.s.l. and inflow limited to $0.03\,m^3\,s^{-1}$. Water abstraction is considered by pumping from node 87 with $400\,L\,s^{-1}$ (see Fig. 7). Three different time periods are considered: (1) steady state, (2) pumping from day 6 to day 38, and (3) recovery from day 38. Beyond the basic model, CADS and conduit-matrix coupling are varied to obtain first insights into sensitivities. Therefore, the CADS width W_{CADS} is set to 0.05 m and 0.50 m (basic model 0.21 m), and the water transfer $\alpha_{ex}/L_{conduit}$ is varied as $4.0 \times 10^{-7}\,m\,s^{-1}$ and $5.0 \times 10^{-7}\,m\,s^{-1}$ (basic model $4.5 \times 10^{-7}\,m\,s^{-1}$).

4.2 Results for the idealized model

In general, water abstraction from the conduit is coupled with a relatively constant drawdown in the pumping well that approaches a plateau with ongoing time (Fig. 8). The matrix drawdown behavior is similar, however, due to the greatly reduced hydraulic conductivity, the process is strongly damped. In principle, CFPM1 with the CADS and FHLQ functionality is able to qualitatively reproduce the field situation described by Maréchal et al. (2008) (Fig. 1). Water budget terms are given in Table 1. Hence, about 10 % of water pumped during period 2 comes from CADS and about 38 % comes from matrix storage. Further model runs are performed to investigate the influence of the CAD storage as well as the conduit-matrix coupling on conduit drawdown. Addition of CAD storage adds fast reacting storage to conduits that allow constantly increasing drawdown. The variation of the CADS results in more (increased CADS) respectively less (reduced CADS) damping of the conduit drawdown as shown in Fig. 8. The amount of pumped water coming from the matrix storage decreases as CADS increases. On the other hand, the amount of pumped water coming from the matrix storage increases as CADS decreases (Table 1), as expected. The smaller the CADS the faster the quasi-steady conduit head is reached (Fig. 8 right). This quasi-steady conduit head depends

on the conduit-matrix coupling as demonstrated by model runs with varying water transfer coefficient (Fig. 8 right). Better conduit-matrix coupling is achieved by higher α_{ex} (conduit-matrix water transfer) values. In fact, drawdowns in the conduit pumping well are reduced with better coupling because the necessary head difference between matrix and conduit to result in a certain water transfer is reduced (see also Eq. 4). On the contrary, smaller water transfer coefficients result in enhanced conduit drawdown. Furthermore, the conduit-matrix coupling does not significantly affect the distribution of water coming from CAD storage and from matrix storage, see Table 1.

5 Conclusions

Implementation of conduit associated drainable (CAD) storage to the existing Conduit Flow Process Mode 1 (CFPM1) combines the conceptual approaches for water storage in karst systems presented by Mangin (1975, 1994) and Drogue (1974, 1992) resulting in a triple porosity system representation (Worthington et al., 2000). CADS considers transient water storage directly connected to the conduit system. The newly developed functionality is fully integrated in the CFPM1 flow subroutines and requires only the storage width as an additional model parameter. The storage width and, therewith, the storage extension can be obtained via transient model calibration.

The CAD storage approach was evaluated in several pumping test scenarios to investigate the effect of storage properties and boundary conditions on karst hydraulics. Simulation results show that associated conduit storage plays a major role during water abstraction from karst systems, even though the majority of total aquifer storage is provided by the matrix storage. This is primarily due to the fact that only little water from matrix storage through conduit-matrix coupling is provided during the early stages of water abstraction. The newly implemented CAD storage flattens the drawdown curve from the beginning of water abstraction from the conduit system because of immediate water inflow from CAD storage.

Depending on the model setup, strong water abstraction within highly permeable structures, i.e. conduits, can result in unhampered water inflow through constant head boundaries connected to the pipe network. This effect leads to minor drawdown during water abstraction even at high pumping rates and consequently an insignificant contribution from the CAD storage. This condition can be relevant, for example, for streams that are hydraulically perfectly connected to karst conduit systems. Therefore, the simulation of pumping tests with CFPM1 requires the additional implementation of a fixed head limited flow (FHLQ) boundary condition, which constrains inflow for constant head boundaries. For these scenarios, water deficit resulting from water abstraction from the conduit system is balanced out by water contribution from the CAD storage and the matrix storage. The presented results show the necessity of transient conduit water storage for simulation of karst hydraulics. Because of the manageable data demand, the newly developed CADS package implemented in CFPM1 can be used for water resources management purposes and evaluation of large scale hydraulic tests for aquifer characterization.

CAD storage and the FHLQ boundary were further evaluated to simulate a scenario representing the large-scale field pumping test reported by Maréchal et al. (2008). Dimensions and hydraulic model parameters were set in the range of observed field values. Even though the geometry of the karst aquifer was highly idealized, the model was able to qualitatively reproduce the overall pattern of drawdown curves observed in the pumping well and the observation wells. However, further comparison of measured drawdown with the so far existent model results is not intended because of the idealized representation of the situation. Ongoing work will evaluate the large-scale pumping test with the modified CFP by using an adequate hydrogeological representation of the catchment and further diagnostic tools like drawdown derivatives and flow dimension analysis. Further work will focus on systematic type curve analyses to evaluate pumping test responses under different complex modeling set-ups.

Acknowledgements. This project was funded by the German Research Foundation (Deutsche Forschungsgemeinschaft – DFG) under Grants No. LI 727/11-2 and GE 2173/2-2. We acknowledge support by the Open Access Publication Funds of the TU Dresden.

References

Ashton, K.: The analysis of flow data from data karst drainage systems, Transactions of the Cave Research Group of Great Britain, 7, 161–203, 1966. 4473

Atkinson, T. C., Smith, D. I., Lavis J. J., and Whitaker, R. J.: Experiments in tracing underground waters in limestone, J. Hydrol., 19, 323–349, 1973. 4465

Bakalowicz, M.: Karst groundwater: a challenge for new resources, Hydrogeol. J., 13, 148–160, doi:10.1007/s10040-004-0402-9, 2005. 4465

Barenblatt, G. I., Zheltov, I. P., and Kochina, I. N.: Basic concepts in the theory of seepage of homogeneous liquids in fissured rock, J. Appl. Math. Mech., 24, 1286–1303, 1960. 4467

Bauer, S., Liedl, R., and Sauter, M.: Modeling the influence of epikarst evolution on karst aquifer genesis: A timevariant recharge boundary condition for joint karst-epikarst development, Water Resour. Res., 41, W09416, doi:10.1029/2004WR003321, 2005. 4469

Birk, S. and Geyer, T.: Prozessbasierte Charakterisierung der dualen Abfluss- und Transporteigenschaften von Karstgrundwasserleitern, Final report DFG project LI 727/10 and SA 501/17, unpublished data, 2006 (in German). 4473

Drogue, C.: Structure de certains aquifères karstiques d'après les résultats de travaux de forage. Comptes Rendus à l'Académie des Sciences de Paris, série III, 278, 2621–2624, 1974. 4465, 4475

Drogue, C.: International Contribution to Hydrogeology 13. Verlag Heinz Heise, Hannover, Germany, 133–149, 1992. 4465, 4475

Ford, D. C. and Williams, P.: Karst hydrogeology and geomorphology, John Wiley & Sons Ltd., West Sussex, 562 pp., 2007. 4466

Geyer, T., Birk, S., Liedl, R., and Sauter, M.: Quantification of temporal distribution of recharge in karst systems from spring hydrographs, J. Hydrol., 348, 452–463, 2008. 4466

Liedl, R., Sauter, M., Hückinghaus, D., Clemens, T., and Teutsch, G.: Simulation of the developmentof karst aquifers using a coupled contiuum pipe flow model, Water Resour. Res., 39, 1–11, 2003. 4466

Mangin, A.: Contribution à l'étude hydrodynamique des aquifères karstiques, Ph.D thesis, Université de Dijon (Annales de Spéléologie, 29, 283–332; 29, 495–601; 30, 21–124, 1975. 4465, 4466, 4475

Mangin, A.: Karst Hydrogeology in groundwater ecology, edited by: Gilbert, J., Danielopol, D. L., and Stanford, J. A., 43–67, Acad. Press San Diego, 1994. 4465, 4475

Maréchal, J. C., Ladouche, B., Dörfliger, N., and Lachassagne, P.: Interpretation of pumping tests in a mixed flow karst system, Water Resour. Res., 44, W05401, doi:10.1029/2007WR006288, 2008. 4465, 4466, 4467, 4468, 4469, 4473, 4474, 4476, 4480, 4481

McDonald, M. G. and Harbaugh, A. W.: A modular three-dimensional finite-difference groundwater flow model: Techniques of Water-Resources Investigations of the United States Geological Survey, Book 6, Chapter A1, 586 pp., 1988. 4466

Reimann, T., Geyer, T., Shoemaker, W. B., Liedl, R., and Sauter, M.: Effects of dynamically variable saturation and matrix-conduit coupling of flow in karst aquifers, Water Resour. Res., 47, W11503, doi:10.1029/2011WR010446, 2011. 4467

Sauter, M., Kovács, A., Geyer, T., and Teutsch, G.: Modellierung der Hydraulik von Karstgrundwasserleitern – Eine Übersicht, Grundwasser, 11, 143–153, 2006. 4466

Shoemaker, W. B., Kuniansky, E. L., Birk, S., Bauer, S., and Swain, E. D.: Documentation of a Conduit Flow Process (CFP) for MODFLOW-2005: U.S. Geological Survey Techniques and Methods, Book 6, Chapter A24, 50 pp., 2008. 4466, 4467

Worthington, S. R. H., Davies, G. J., and Ford, D. C.: Matrix, fracture and channel components of storage and flow in a Paleozoic limestone aquifer, in Groundwater flow and contaminant transport in carbonate aquifers, edited by: Sasowsky, I. D. and Wicks, C. M., 113–128, Balkema, Rotterdam, 2000. 4465, 4466, 4475

Worthington, S. R. H.: Groundwater residence times in unconfined carbonate aquifers, J. Cave Karst Stud., 69, 94–102, 2007. 4466

Table 1. Water budget terms for CFPM1 demonstrating the origin of pumped water. All terms are computed based on average values for period 2.

MODELRUN	BASIC	CADS (⇓)	CADS (⇑)	α_{ex} (⇓)	α_{ex} (⇑)
spring (FHLQ boundary)	7.5 %	7.5 %	7.5 %	7.5 %	7.5 %
CADS	9.9 %	2.4 %	21.2 %	11.5 %	8.6 %
matrix (all terms)	82.6 %	90.1 %	71.3 %	81.0 %	83.9 %
matrix: from storage	38.2 %	44.0 %	29.0 %	39.3 %	37.0 %
matrix: from recharge	47.1 %	47.1 %	47.1 %	47.1 %	47.1 %
matrix: from river	15.8 %	16.8 %	14.6 %	14.0 %	17.5 %
matrix: to storage	0.0 %	0.0 %	0.0 %	0.0 %	0.0 %
matrix: to river	−18.5 %	−17.8 %	−19.4 %	−19.4 %	−17.7 %

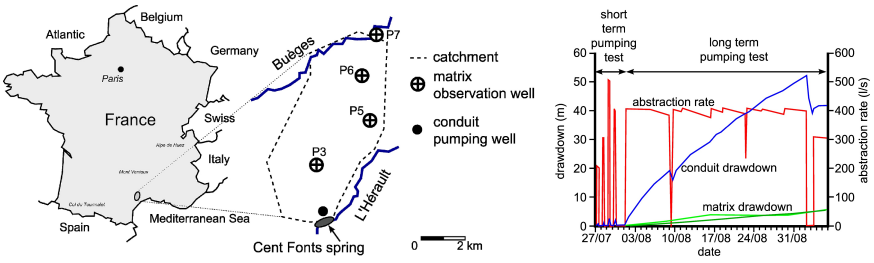

Fig. 1. Left: schematic sketch of the Cent Fonts catchment, where a large scale and long term pumping test was conducted (Maréchal et al., 2008); right: abstraction rate and drawdown in both matrix and conduit for a long term and large scale pumping test; figures from Maréchal et al. (2008).

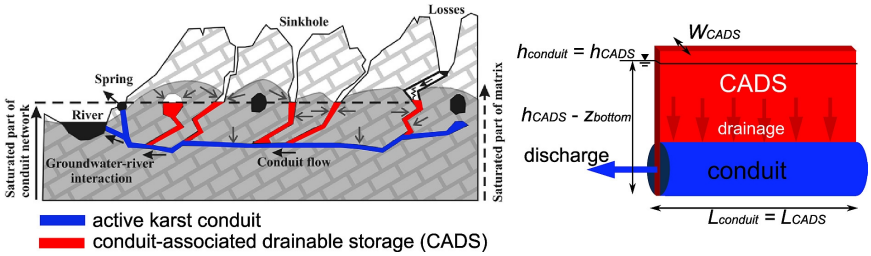

Fig. 2. Conceptual implementation of CAD storage for a karst catchment, left figure from Maréchal et al. (2008).

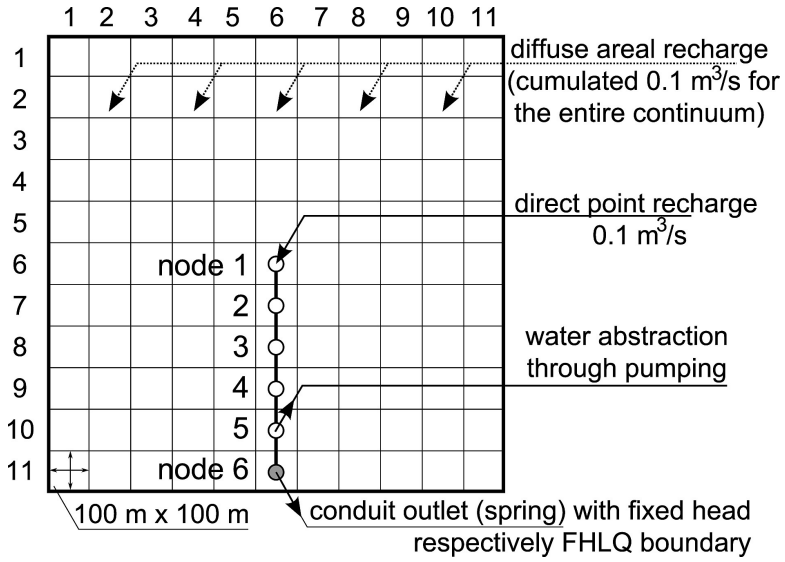

Fig. 3. Sketch of the model setup used for testing the CADS and FHLQ functionality.

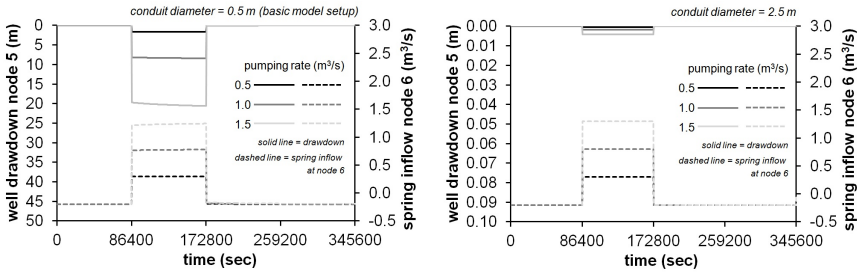

Fig. 4. Conduit head at the pumping well and inflow via conduit constant head boundary condition for different pumping rates; left: *conduit diameter = 0.5 m* (basic model setup), right: *conduit diameter = 2.5 m*.

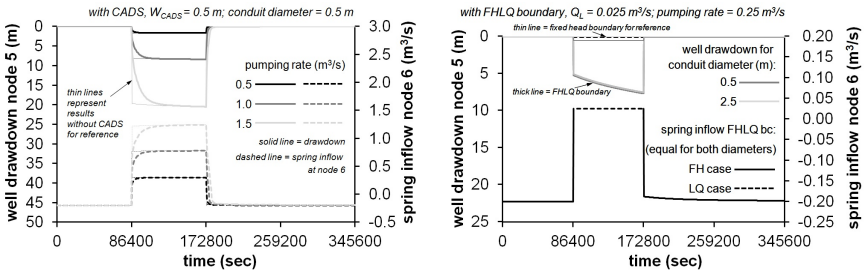

Fig. 5. Left: use of CADS – conduit head at the pumping well and inflow via conduit constant head boundary for different pumping rates; right: use of FHLQ boundary – conduit head at the pumping well and inflow via karst spring for different conduit diameters (pumping rate = 0.25 $m^3 s^{-1}$; please note different scales on the y-axes).

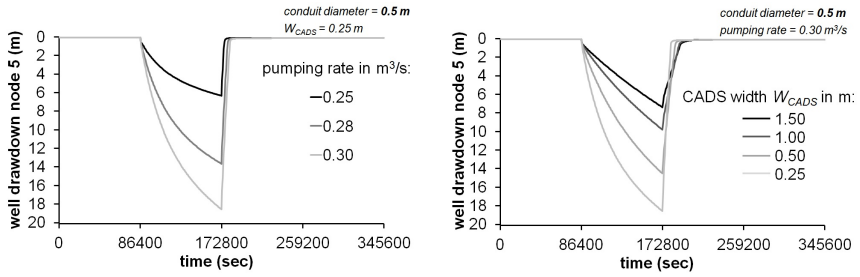

Fig. 6. Left: conduit head at the pumping well for different pumping rates for a conduit with D = 0.5 m; right: conduit head at the pumping well for different CAD storage representations for a conduit with D = 0.5 m.

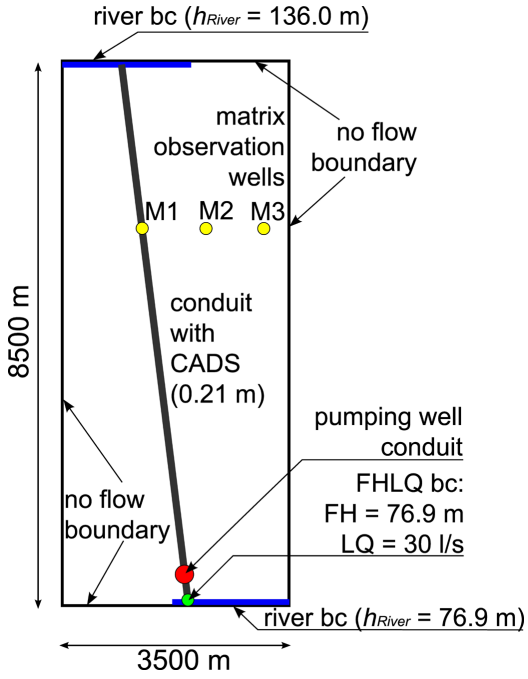

Fig. 7. Conceptual representation of the large scale pumping test scenario.

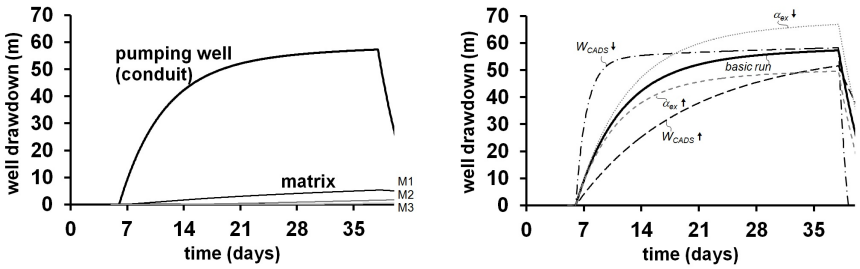

Fig. 8. Left: computed drawdown in both conduit and matrix for the basic situation; right: computed drawdown in the conduit for varying CADS width and water transfer coefficient.